POLITECNICO DI TORINO
Repository ISTITUZIONALE

A Numerical Verification of Analytical Solution for the Mixed Fourier Transform Equation

Original
A Numerical Verification of Analytical Solution for the Mixed Fourier Transform Equation / Petek, Martin; Tihon, Denis; Tobon, Jorge; Craeye, Christophe; Vipiana, Francesca. - (2025), pp. 1-5. (19th European Conference on Antennas and Propagation, EuCAP 2025 Stockholm (Sve) 30 March 2025 - 04 April 2025) [10.23919/eucap63536.2025.10999455].

Availability:
This version is available at: 11583/3010838 since: 2026-05-15T12:34:56Z

Publisher:
IEEE

Published
DOI:10.23919/eucap63536.2025.10999455

Terms of use:

This article is made available under terms and conditions as specified in the corresponding bibliographic description in the repository

Publisher copyright
IEEE postprint/Author's Accepted Manuscript

©2025 IEEE. Personal use of this material is permitted. Permission from IEEE must be obtained for all other uses, in any current or future media, including reprinting/republishing this material for advertising or promotional purposes, creating new collecting works, for resale or lists, or reuse of any copyrighted component of this work in other works.

(Article begins on next page)

23 May 2026

A Numerical Verification of Analytical Solution for the Mixed Fourier Transform Equation

Martin Petek*, Denis Tihon†, Jorge Alberto Tobón Vásquez*, Christophe Craeye†, Francesca Vipiana*,
*Dept. of Electronics and Telecommunications, Politecnico di Torino, 10129, Torino, Italy, martin.petek@polito.it
†ICTEAM Institute, Université catholique de Louvain (UCLouvain), Louvain-la-Neuve, Belgium.

***Abstract*—Analysis of 2D-periodic structures is often carried out with the Method of Moments, which is capable to obtain simultaneously the phase velocity and attenuation constant of surface- or leaky-waves (i.e. eigenmodes). However, to find the eigenmodes associated with a given geometry, many samples of the impedance matrix are needed, whose evaluation can be computationally expensive. To overcome the computational burden, efficient interpolation procedures have been proposed, which are based on the decomposition of the impedance matrix into Floquet modes and the proper extraction of some of them. However, the evaluation of a given Floquet mode with the reaction integral can be difficult when the integration regions of the source and test basis functions overlap along the z-axis. In this work, we deal with this difficult case: we propose a fully analytical solution and validate it numerically. Our work paves the way to the generalization of existing fast interpolation procedures to arbitrary structures and, eventually, to the fast analysis of general 2D-periodic geometries.**

***Index Terms*—periodic structures, metasurfaces, method of moments**

I. Introduction

Periodic structures find many uses in antenna engineering and are therefore frequently implemented, for example as antenna arrays [1], metasurfaces [2], [3], reconfigurable intelligent surfaces [4], and electromagnetic bandgap materials [5], [6]. For the analysis of periodic structures, the Method of Moments (MoM) is frequently employed, for example in [6]–[10].

Recently, some of the authors have proposed an MoM modelling procedure [10], especially tailored for glide-symmetric structures. The MoM was able to robustly yield the source-free solutions and is capable of evaluating the stopband attenuation. However, its main drawback is the search for resonances of the structure as singularities of the impedance matrix, which can be prohibitively expensive if each impedance matrix is directly computed. This computation can be accelerated with the use of interpolation schemes, as is done in other works [6], [11], [12]. In a recent paper [12] of some of the authors, the behaviour of the interaction between two impedance matrix elements is regularized by extracting the first few Floquet modes, which are difficult to interpolate. These are then re-added after interpolation. However, the formulation is valid only when there exists no vertical component in the basis functions (BF) and is therefore not applicable to non-planar geometries.

In this work, we present preliminary results for an interpolation method based on [12], which is applicable to 3D geometries. Specifically, we present an analytical solution to the interaction between two Rao-Wilton-Glisson (RWG) BF which may overlap along the z-axis. The solution is validated with the help of a custom quadrature scheme. This development is key in developing a fast interpolation technique for general geometries, and could pave the way to dramatically speed up any periodic MoM problem.

II. Derivation of Analytical equation

In general, a single impedance matrix element interaction can be computed in the spectral domain as [13]:

$$Z(\mathbf{k}_{t00}) = -\frac{\eta_d}{k_d}\frac{1}{S_{u.c.}}\sum_{mn}\frac{1}{2k_z^{mn,+}} \\ k_d^2\iint_{\mathbf{r}} c_{\mathrm{t}}\mathbf{f}_{\mathrm{t}}(\mathbf{r})\cdot\mathbf{J}^{\perp}_{u.c.}(\mathbf{k}_t^{mn,\pm}|z)\exp(-j\mathbf{k}^{mn,\pm}\cdot\mathbf{r})\,\mathrm{d}\mathbf{r}, \quad (1)$$

where k_d and η_d are the wave vector and impedance in free space, $S_{u.c}$ is the area of the unit cell, and $\mathbf{f}_{\mathrm{t}}$ is the test basis function $\mathbf{r}$ is the observation (test) position vector. The integration is done over the support of the test basis function. The wave vector $\mathbf{k}^{mn,\pm}$ is obtained as

$$\mathbf{k}^{mn,\pm} = \mathbf{k}_t^{mn} \pm \hat{\mathbf{z}}\sqrt{k_d^2 - \mathbf{k}_t^{mn}\cdot\mathbf{k}_t^{mn}}\,, \quad (2)$$

where the m and n are the indices of the Floquet mode with its transverse wave vector $\mathbf{k}_t^{mn}$:

$$\mathbf{k}_t^{mn} = \mathbf{k}_{t00} + m\frac{2\pi(\mathbf{s}_2\times\hat{\mathbf{z}})}{S_{u.c.}} + n\frac{2\pi(\hat{\mathbf{z}}\times\mathbf{s}_1)}{S_{u.c.}}\,. \quad (3)$$

The value of $\mathbf{k}_{t00}$ is a freely chosen simulation parameter and may take complex values. The choice of the correct branch $\pm$, and therefore the value of $\mathbf{J}^{\perp}_{u.c.}$ depends whether z' is below or above z:

$$\mathbf{J}^{\perp}_{u.c.}(\mathbf{k}^{\pm}|z) = \iint_{\{\mathbf{r}'|\pm z'<\pm z\}}\mathbf{f}_{\mathrm{s}}^{\perp}(\mathbf{r}',\mathbf{k}^{\pm})\exp(j\mathbf{k}^{\pm}\cdot\mathbf{r}')\,\mathrm{d}\mathbf{r}'\,, \quad (4)$$

where the $\mathbf{f}_{\mathrm{s}}^{\perp}$ is the component of $\mathbf{f}_{\mathrm{s}}$ transversal to $\hat{\mathbf{k}}^{\pm}$

$$\mathbf{f}_{\mathrm{s}}^{\perp}(\mathbf{r}',\mathbf{k}^{\pm}) = c_{\mathrm{s}}\mathbf{f}_{\mathrm{s}}(\mathbf{r}') - \left(c_{\mathrm{s}}\mathbf{f}_{\mathrm{s}}(\mathbf{r}')\cdot\hat{\mathbf{k}}^{\pm}\right)\hat{\mathbf{k}}^{\pm}\,. \quad (5)$$

For $z<z'$, we must choose the " $-$ " branch and for $z>z'$ the " $+$ " branch of the equation. This branch choice is the core of the problem discussed in this paper. It arises due to the condition that the electric field, created by a source at z',

vanishes as z tends towards infinity. In (5), $\hat{\mathbf{k}}^{\pm} = \mathbf{k}/k_d$, and $\mathbf{f}_\mathrm{s}$ is the source BF. Both $\mathbf{f}_\mathrm{s}$ and $\mathbf{f}_\mathrm{t}$ in this work are the unnormalized RWG BF [14]:

$$c_{\mathrm{t/s}}\mathbf{f}_{\mathrm{t/s}}(\mathbf{r}) = \begin{cases} c^{+}_{\mathrm{t/s}}(\mathbf{r}-\mathbf{r}^{+}_{\mathrm{v,t/s}}), & \text{if } \mathbf{r} \text{ on } + \text{ triangle} \\ c^{-}_{\mathrm{t/s}}(\mathbf{r}-\mathbf{r}^{-}_{\mathrm{v,t/s}}), & \text{if } \mathbf{r} \text{ on } - \text{ triangle} \\ \mathbf{0}, & \text{if } \mathbf{r} \text{ elsewhere} \end{cases}, \tag{6}$$

where the $c_{\mathrm{t/s}}$ is a normalization coefficient of RWG and $\mathbf{r}_{\mathrm{v,t/s}} = \{x_{\mathrm{v,t/s}}, y_{\mathrm{v,t/s}}, z_{\mathrm{v,t/s}}\}$ is the position vector to the vertex opposite to the shared edge. In the following discussion, we will focus on a single pair of source and test triangles, as the solutions are identical for both $+$ and $-$ triangles.

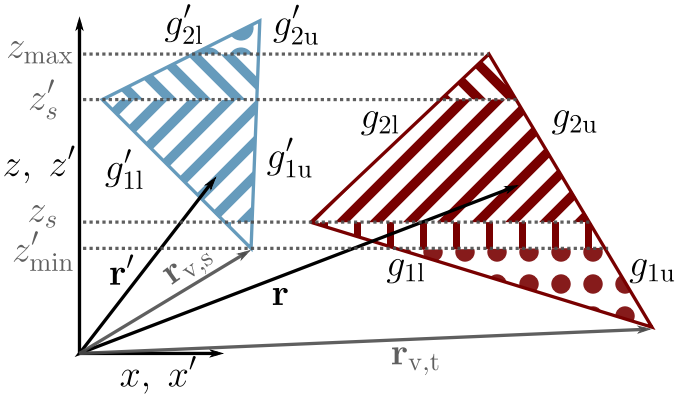

Fig. 1. Interaction between the test and the source triangles. The overlapping regions are presented with stripes. The non overlapping regions are presented with dots.

In obtaining an analytic equation for (1), the main challenge occurs when there are regions of source and test triangles which overlap. Since we must always select the positive branch of the equation when $z' < z$, and the negative branch when $z' > z$, the integrals are not separable. We treat the integration in the following manner. First, we parameterize the triangles in the xz-plane, depicted in Fig. 1. Therefore,

$$y = a_1 x + a_2 z + a_3, \qquad y' = a'_1 x' + a'_2 z' + a'_3. \tag{7}$$

Note that the parametrization above is valid for almost all orientations of the triangles, except if their normals are aligned with the $\hat{\mathbf{x}}$ or $\hat{\mathbf{z}}$. Then, we split the integral in both z and z' at the middle vertices, here defined as z_s for the test and z'_s for the source triangle. This situation is presented in Fig. 1. As can be seen from the figure, the integration region along x and x' is bound by the linear functions

$$g(z) = sz + n, \qquad g'(z') = s'z' + n', \tag{8}$$

where the subscripts l and u denote the lower and upper boundary and indices indicate the change of the slope s and offset n. Depending on the triangle geometry, at least two of the equations are equal ($g_{2\mathrm{u}} = g_{1\mathrm{u}}$ and $g'_{2\mathrm{u}} = g'_{1\mathrm{u}}$ in Fig. 1). Next, we subdivide the region of integration in z and z' by splitting the triangles, such that the vertices of the test triangle split the integration along z' of the source triangle and vice-versa, presented in dashed lines in Fig. 1.

We have thus split each triangle in smaller subdivisions, where boundaries are clearly defined for both source and test integration. Furthermore, for each subregion of the source triangle, there is at most one corresponding subregion of the test triangle where the integration domains of z and z' overlap ("mixed" subregions), for the rest either $z \leq z'$ or $z \geq z'$ ("separable" subregions), as depicted in Fig. 1. For any two subregions, the integral in (1) is:

$$K \int_{z_1}^{z_2} \mathrm{d}z \int_{g_l(z)}^{g_u(z)} \mathrm{d}x\, \exp(-j\mathbf{k}^{\pm}\cdot\mathbf{r})\mathbf{f}_\mathrm{t}(\mathbf{r})\cdot \left[K' \int_{z'_1}^{z'_2} \mathrm{d}z' \int_{g'_l(z')}^{g'_u(z')} \mathrm{d}x'\, \mathbf{f}^{\perp}_\mathrm{s}(\mathbf{r}', \mathbf{k}^{\pm}) \exp(j\mathbf{k}^{\pm}\cdot\mathbf{r}')\right], \tag{9}$$

with $K = c_\mathrm{t}\sqrt{1+a_1^2+a_2^2}$ and $K' = c_\mathrm{s}\sqrt{1+a_1'^2+a_2'^2}$.

In the following subsections, we shall provide the derived expressions for both separable and mixed subregions. The end result can then be obtained by carefully summing the solution for interaction of individual subregions. By analyzing (9), we see that a key integral identity is a polynomial multiplied with an exponential function:

$$\int (c_1\xi^2 + c_2\xi + c_3)\exp(c_4\xi + c5)\,\mathrm{d}\xi = \text{const.} + \frac{1}{c_4^3}\big(c_1(2-2c_4\xi+c_4^2\xi^2)+c_4(c_3c_4+c_2(c_4\xi-1)\big)\exp(c_4\xi+c_5)\,. \tag{10}$$

As can be seen from (10), the integration results in the same kind of function. Therefore, the multiple integrals can be done with a repeated use of the integral identity and careful tracking of constants. For brevity of this paper, a detailed derivation shall be omitted.

A. Separable regions

This formulation is applicable in cases where the intervals of integration in z' and z do not overlap, that is all regions with a different pattern for striped patterns in Fig. 1, or the complete other triangle for regions with a dotted pattern (which do not overlap at any point). For two subregions Δ'_b of the source and Δ_a of the test triangles, depicted in Fig. 2, the integrals can be computed independently from one another:

$$I^{\Delta_a \leftrightarrow \Delta'_b}_{\mathrm{total}} = \mathbf{I}^{\Delta_a}_{\mathrm{d}x\mathrm{d}z} \cdot \mathbf{I}^{\Delta'_b}_{\mathrm{d}x'\mathrm{d}z'}\,. \tag{11}$$

Here, $\mathbf{I}^{\Delta_a}_{\mathrm{d}x\mathrm{d}z}$ can be obtained with solving the integral:

$$\mathbf{I}^{\Delta_a}_{\mathrm{d}x\mathrm{d}z} = K \iint_{\mathbf{r}\in\Delta_a} \mathbf{f}_\mathrm{t}(\mathbf{r}) \exp(-j\mathbf{k}^{mn,\pm}\cdot\mathbf{r})\,\mathrm{d}\mathbf{r}\,, \tag{12}$$

whereas $\mathbf{I}^{\Delta'_b}_{\mathrm{d}x'\mathrm{d}z'}$ can be obtained with:

$$\mathbf{I}^{\Delta'_b}_{\mathrm{d}x'\mathrm{d}z'} = K' \iint_{\mathbf{r}\in\Delta'_b} \mathbf{f}^{\perp}_\mathrm{s}(\mathbf{r}', \mathbf{k}^{mn,\pm}) \exp(j\mathbf{k}^{mn,\pm}\cdot\mathbf{r}')\,\mathrm{d}\mathbf{r}'\,. \tag{13}$$

For a given region with $z \in [z_1, z_2]$ and $x \in [g_l(z), g_u(z)]$, presented in Fig. 2, the test integral (12) can be obtained with:

$$\mathbf{I}^{\Delta_a}_{\mathrm{d}x\mathrm{d}z} = \mathbf{I}_{\mathrm{d}x\mathrm{d}z}(z_2 \,|\, g_\mathrm{u}) - \mathbf{I}_{\mathrm{d}x\mathrm{d}z}(z_1 \,|\, g_\mathrm{u}) - \mathbf{I}_{\mathrm{d}x\mathrm{d}z}(z_2 \,|\, g_\mathrm{l}) + \mathbf{I}_{\mathrm{d}x\mathrm{d}z}(z_1 \,|\, g_\mathrm{l})\,, \tag{14}$$

where a single part is given by

$$\mathbf{I}_{\mathrm{d}x\mathrm{d}z}(z \,|\, g) = \Big[\hat{\mathbf{x}}(sz + A_{11} - s/A_{14}) + \hat{\mathbf{y}}(A_{12}z + A_{13} - A_{12}/A_{14}) + \hat{\mathbf{z}}(z - z_{\mathrm{v,t}} - A_{14}^{-1})\Big] \frac{\exp(A_{14}z + A_{15})}{A_1 A_{14}} \,. \quad (15)$$

Here, $z_{\mathrm{v,t}}$ is the z-component of the $\mathbf{r}_{\mathrm{v,t}}$ for the test BF and the constants, which are a function of the integration boundary g and the wave-vector, are given by:

$$A_1 = -j(k_x + k_y a_1) \quad (16)$$
$$A_{11} = n - x_{\mathrm{v,t}} - A_1^{-1} \quad (17)$$
$$A_{12} = a_1 s + a_2 \quad (18)$$
$$A_{13} = a_1 n + a_3 - y_{\mathrm{v,t}} - a_1/A_1 \quad (19)$$
$$A_{14} = A_1 s - j(k_y a_2 + k_z) \quad (20)$$
$$A_{15} = A_1 n - j k_y a_3 \,. \quad (21)$$

The source integral is given by:

$$\mathbf{I}^{\Delta'_b}_{\mathrm{d}x'\mathrm{d}z'} = \mathbf{I}'_{\mathrm{d}x'\mathrm{d}z'}(z'_2 \,|\, g'_{\mathrm{u}}) - \mathbf{I}'_{\mathrm{d}x'\mathrm{d}z'}(z'_1 \,|\, g'_{\mathrm{u}}) - \mathbf{I}'_{\mathrm{d}x'\mathrm{d}z'}(z'_2 \,|\, g'_{\mathrm{l}}) + \mathbf{I}'_{\mathrm{d}x'\mathrm{d}z'}(z_1 \,|\, g'_{\mathrm{l}}) \,, \quad (22)$$

where the indefinite integral is:

$$\mathbf{I}'_{\mathrm{d}x'\mathrm{d}z'}(z' \,|\, g') = \Big[\hat{\mathbf{x}}(B_{16}z + B_{17}) + \hat{\mathbf{y}}(B_{18}z + B_{19}) + \hat{\mathbf{z}}(B_{20}z + B_{21})\Big] \frac{\exp(B_{14}z + B_{15})}{B_7 B_{14}} \,. \quad (23)$$

The constants in (23) are:

$$B_1 = \hat{k}_x + \hat{k}_y a'_1 \quad (24)$$
$$B_2 = \hat{k}_y a'_2 + \hat{k}_z \quad (25)$$
$$B_3 = -x_{\mathrm{v,s}}\hat{k}_x + (a'_3 - y_{\mathrm{v,s}})\hat{k}_y - z_{\mathrm{v,s}}\hat{k}_z \quad (26)$$
$$B_4 = 1 - \hat{k}_x B_1 \quad (27)$$
$$B_5 = a'_1 - \hat{k}_y B_1 \quad (28)$$
$$B_6 = -\hat{k}_z B_1 \quad (29)$$
$$B_7 = j(k_x + k_y a'_1) \quad (30)$$
$$B_8 = B_{16} = B_4 s' - \hat{k}_x B_2 \quad (31)$$
$$B_9 = B_4 n' - x_{\mathrm{v,s}} - \hat{k}_x B_3 - B_4/B_7 \quad (32)$$
$$B_{10} = B_{18} = B_5 s' + (a'_2 - \hat{k}_y B_2) \quad (33)$$
$$B_{11} = B_5 n' + a'_3 - y_{\mathrm{v,s}} - \hat{k}_y B_3 - B_5/B_7 \quad (34)$$
$$B_{12} = B_{20} = B_6 s' + 1 - \hat{k}_z B_2 \quad (35)$$
$$B_{13} = B_6 n' - z_{\mathrm{v,s}} - \hat{k}_z B_3 - B_6/B_7 \quad (36)$$
$$B_{14} = B_7 s' + j(k_y a'_2 + kz) \quad (37)$$
$$B_{15} = B_7 n' + j k_y a'_3 \quad (38)$$
$$B_{17} = B_9 - B_8/B_{14} \quad (39)$$
$$B_{19} = B_{11} - B_{10}/B_{14} \quad (40)$$
$$B_{21} = B_{13} - B_{12}/B_{14} \,. \quad (41)$$

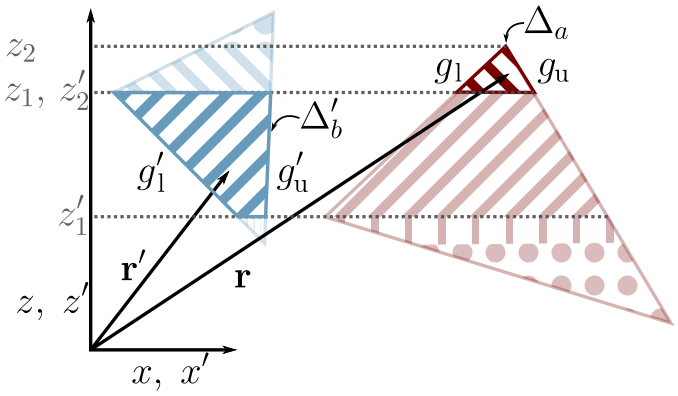

Fig. 2. Computing interaction between two separated subregions.

B. Mixed regions

Consider the example of overlapping regions in Fig. 3. The region of integration over the source triangle is Δ'_a, bounded by z'_1 and z'_2 and linear functions g'_l and g'_u, and analogously for the test triangle.

For such subregions, the integrals in (9) are not separable in z and z'. Therefore, we can first integrate along x and x', since these directions are orthogonal to z and z'. Remaining is a double integral in z and z'. We ensure the correct choice of the $\pm$ branch by further splitting this integration along z' into two subregions $z' = [z'_1, z]$ and $z' = [z, z'_2]$. Interestingly, in that case, an analytical solution can be found; it makes use of some of the constants already developed for the separable case (constants A and B). The solution reads as:

$$I^{\Delta_a \leftrightarrow \Delta'_a}_{\mathrm{total}} = \mathbf{I}^{\Delta_a}_{\mathrm{d}x\mathrm{d}z} \cdot \Big(\mathbf{I}'_{\mathrm{d}x'\mathrm{d}z'}(z'_1 \,|\, g'_{\mathrm{l}}) - \mathbf{I}'_{\mathrm{d}x'\mathrm{d}z'}(z'_1 \,|\, g'_{\mathrm{u}})\Big) + \mathrm{II}'^{\Delta_a \leftrightarrow \Delta'_a} \,, \quad (42)$$

where the first part of the equation is obtained through (14) and (23) and the second part by

$$\begin{aligned}\mathrm{II}'^{\Delta_a \leftrightarrow \Delta'_a} =& \mathrm{II}'_\delta(z_2, z'_2 \,|\, g_u, g'_u) + \mathrm{II}'_\delta(z_2, z'_1 \,|\, g_l, g'_l) - \\ & \mathrm{II}'_\delta(z_2, z'_2 \,|\, g_l, g'_u) - \mathrm{II}'_\delta(z_2, z'_1 \,|\, g_u, g'_l) - \\ & \mathrm{II}'_\delta(z_1, z'_2 \,|\, g_u, g'_u) - \mathrm{II}'_\delta(z_1, z'_1 \,|\, g_l, g'_l) + \\ & \mathrm{II}'_\delta(z_1, z'_2 \,|\, g_l, g'_u) + \mathrm{II}'_\delta(z_1, z'_1 \,|\, g_u, g'_l) \,.\end{aligned} \quad (43)$$

Note that the indefinite integral $\mathrm{II}'_\delta(z, z' \,|\, g, g')$ is a scalar value. Its equation is:

$$\mathrm{II}'_\delta(z, z' \,|\, g, g') = \frac{\exp(C_4 z + C_5)}{A_1 B_7 B_{14} C_4^3} \Big(C_1\big(2 - 2C_4 z + C_4^2 z^2\big) + C_4\big(C_3 C_4 + C_2(C_4 z - 1)\big)\Big) \,, \quad (44)$$

where the constants A and B are given in the previous section, and the other ones are defined as:

$$C_1 = A_{12}B_{18} + B_{20} + B_{16}s \tag{45}$$
$$C_2 = C_{2,\delta} + B_{17}s - B_{20}z_{\mathrm{v,t}} \tag{46}$$
$$C_{2,\delta} = A_{11}B_{16} + A_{13}B_{18} + A_{12}B_{19} + B_{21} \tag{47}$$
$$C_3 = A_{11}B_{17} + A_{13}B_{19} - B_{21}z_{\mathrm{v,t}} \tag{48}$$
$$C_4 = A_{14} + B_{14} \tag{49}$$
$$C_5 = A_{15} + B_{15}\ . \tag{50}$$

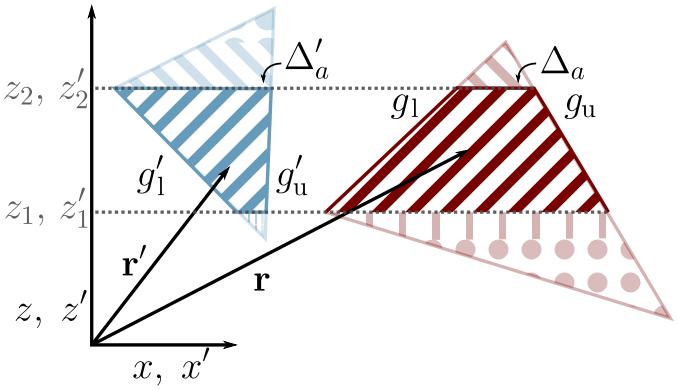

Fig. 3. Computing interaction between two overlapping subregions.

III. Validation of Analytical Equation

To validate the developed analytical solution, we can compare the analytical results with a numerically obtained result. However, since the integral (9) contains a branch cut, and we want to obtain a highly accurate reference, it is not sufficient to directly apply a quadrature rule to the two triangular regions. Instead, we subdivide them into subregions of integration, as is done in Fig. 1. In case the subregion is a quadrilateral, it is further split into four triangles at the barycenter. Then, each triangular subregion is integrated separately using Gauss-Legendre quadrature [15] and the partial results are summed up to obtain the complete interaction.

We will now compare the results for the analytical equation from Sec. II for the two geometries in Fig. 4 and Tab. I, and the simulation parameters from Tab. II. The results for the geometry in Fig. 4(a) are presented in Fig. 5. The figure presents significant digits of the analytical equation, obtained with double (a) and quad (b) precision for different Floquet mode indices m and n in (3). Here, the double precision solves the analytical equation with a sufficient accuracy (above 3 digits of precision) for all Floquet indices, although there are some where a loss of significant digits is observed.

The results for the geometry in Fig. 4(b) are presented in Fig. 6. There is an excellent agreement when quad precision is used, but in the case of a double precision we observe a great loss of significant digits. For the region with indices $n = 0$ and $n = -1$, the loss is critical as the analytical solution (evaluated in double precision) is correct to less than two

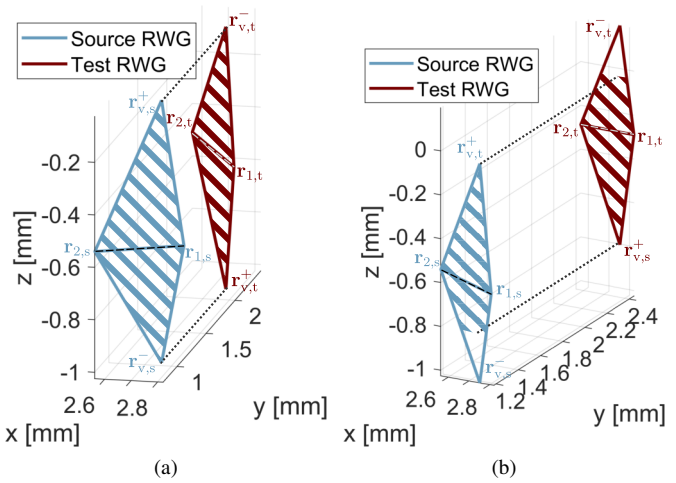

Fig. 4. Studied geometries, the overlapped regions are shown in stripes. The vertice positions are presented in Tab. I. (a): Geometry 1, BF completely overlap and are not aligned with $\hat{\mathbf{y}}$. (b): Geometry 2, BF partially overlap and are aligned with $\hat{\mathbf{y}}$.

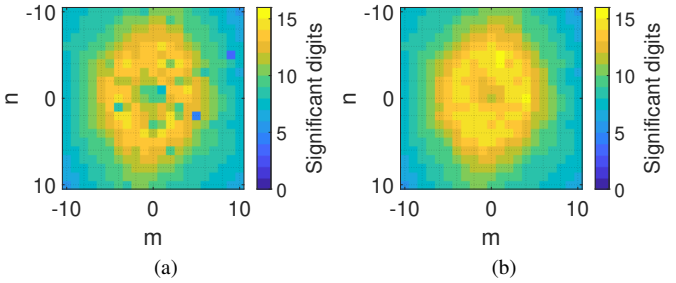

Fig. 5. Correct significant digits of the analytical equation. The reference is the custom quadrature. Computed in: (a) double precision (b) quad precision.

significant digits. Most likely, this is caused by the analytical equation consisting of many subtractions, which results in a difference of two almost equal large numbers. This kind of dramatic cancellation effect are typically encountered when dealing with peculiar geometries and solving analytically high-dimensional integrals. However, there exist several techniques to mitigate the problem, which will be investigated in a future work.

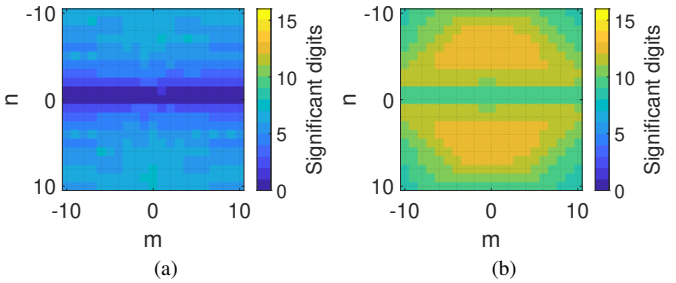

Fig. 6. Correct significant digits of the analytical equation. The reference is the custom quadrature. Computed in: (a) double precision (b) quad precision.

Finally, we will now compare the simulation time of the two integration techniques. The time to solve a single integral with the quadrature rule in double precision is 0.31 s, while the analytical equation is solved in $1.6 \cdot 10^{-3}$ s with double

precision, and 4.2 s with quad precision. The extremely rapid solution of the analytical equation motivates future efforts for improving this work.

TABLE I
POSITION OF VERTICES FOR BFS FOR GEOMETRY 1 (LEFT) AND GEOMETRY 2 (RIGHT).

Vertice	Value (case 1) $\{x, y, z\}$ [mm]
$\mathbf{r}^{+}_{\mathrm{v,s}}$	$\{2.7532, 1.0446, -0.025\}$
$\mathbf{r}_{1,\mathrm{s}}$	$\{2.8085, 1.1782, -0.6098\}$
$\mathbf{r}_{2,\mathrm{s}}$	$\{2.5639, 0.7578, -0.5398\}$
$\mathbf{r}^{-}_{\mathrm{v,s}}$	$\{2.7532, 1.0446, -1.0250\}$
$\mathbf{r}^{+}_{\mathrm{v,t}}$	$\{2.7532, 2.1554, -1.0250\}$
$\mathbf{r}_{1,\mathrm{t}}$	$\{2.5634, 2.4427, -0.5097\}$
$\mathbf{r}_{2,\mathrm{t}}$	$\{2.8215, 1.9825, -0.5115\}$
$\mathbf{r}^{-}_{\mathrm{v,t}}$	$\{2.7532, 2.1554, -0.025\}$

Vertice	Value (case 2) $\{x, y, z\}$ [mm]
$\mathbf{r}^{+}_{\mathrm{v,s}}$	$\{2.7532, 1.1782, -0.025\}$
$\mathbf{r}_{1,\mathrm{s}}$	$\{2.8085, 1.1782, -0.6098\}$
$\mathbf{r}_{2,\mathrm{s}}$	$\{2.5639, 1.1782, -0.5399\}$
$\mathbf{r}^{-}_{\mathrm{v,s}}$	$\{2.7532, 1.1782, -1.0250\}$
$\mathbf{r}^{+}_{\mathrm{v,t}}$	$\{2.7532, 2.4427, -0.8033\}$
$\mathbf{r}_{1,\mathrm{t}}$	$\{2.8085, 2.4427, -0.2880\}$
$\mathbf{r}_{2,\mathrm{t}}$	$\{2.5639, 2.4427, -0.2899\}$
$\mathbf{r}^{-}_{\mathrm{v,t}}$	$\{2.7532, 2.4427, 0.1967\}$

TABLE II
SIMULATION PARAMETERS.

Parameter	Meaning	Value
$\mathbf{k}_{\mathrm{t}00}$	transverse wave vector	$\{\pi/\|\|s_1\|\|, \pi/(2\|\|s_1\|\|), 0\}$
$\mathbf{s}_1$	period in x	$3.2\,\hat{\mathbf{x}}$ mm
$\mathbf{s}_2$	period in y	$3.2\,\hat{\mathbf{y}}$ mm
f	frequency	10 GHz

IV. CONCLUSIONS AND FUTURE WORK

This work has presented preliminary results for a fast interpolation scheme for interaction between two RWG BFs in a periodic structure. A key result is the development of a fully analytical solution of the reaction integral in the spectral form between two RWG BF. The analytical equation has been validated with the use of a custom quadrature. The results indicate a good agreement of the analytical and the numerical solutions, although a loss of accuracy is observed in some cases where double precision is used.

The future work consists of generalizing the derivation to arbitrary orientations of the two triangles, developing a more stable formulation and implementing it in an interpolation scheme.

ACKNOWLEDGMENT

This publication is based upon work from the Horizon Europe Research and Innovation Program and UKRI under the GENIUS Project, Marie Skłodowska-Curie Grant under Agreement 101072560, and in part by the project PON Research and Innovation "Microwave Imaging and Detection powered by Artificial Intelligence for Medical and Industrial Applications (DM 1062/21)," funded by the MUR, and in part by the project "MedWaveImage - Microwave imaging technology transfer to innovate the medical sector", funded by Interreg Central Europe (CE0200670). It is also supported by Unite! – University Network for Innovation, Technology and Engineering.

REFERENCES

[1] J. P. Doane, K. Sertel, and J. L. Volakis, "A Wideband, Wide Scanning Tightly Coupled Dipole Array With Integrated Balun (TCDA-IB)," *IEEE Transactions on Antennas and Propagation*, vol. 61, no. 9, pp. 4538–4548, 2013.

[2] O. Quevedo-Teruel, J. Miao, M. Mattsson, A. Algaba-Brazalez, M. Johansson, and L. Manholm, "Glide-Symmetric Fully Metallic Luneburg Lens for 5G Communications at Ka-Band," *IEEE Antennas and Wireless Propagation Letters*, vol. 17, no. 9, pp. 1588–1592, 2018.

[3] M. Faenzi, D. González-Ovejero, G. Petraglia, G. D'Alterio, F. Pascariello, R. Vitiello, and S. Maci, "A Metasurface Radar Monopulse Antenna," *IEEE Transactions on Antennas and Propagation*, vol. 70, no. 4, pp. 2571–2579, 2022.

[4] Y. Feng, Q. Hu, K. Qu, W. Yang, Y. Zheng, and K. Chen, "Reconfigurable Intelligent Surfaces: Design, Implementation, and Practical Demonstration," *Electromagnetic Science*, vol. 1, no. 2, pp. 1–21, 2023.

[5] A. U. Zaman and P.-S. Kildal, "Wide-Band Slot Antenna Arrays With Single-Layer Corporate-Feed Network in Ridge Gap Waveguide Technology," *IEEE Transactions on Antennas and Propagation*, vol. 62, no. 6, pp. 2992–3001, 2014.

[6] A. Barlevy and Y. Rahmat-Samii, "Characterization of electromagnetic band-gaps composed of multiple periodic tripods with interconnecting vias: concept, analysis, and design," *IEEE Trans. Antennas Propag.*, vol. 49, no. 3, pp. 343–353, 2001.

[7] J. Budhu and A. Grbic, "Perfectly Reflecting Metasurface Reflectarrays: Mutual Coupling Modeling Between Unique Elements Through Homogenization," *IEEE Transactions on Antennas and Propagation*, vol. 69, no. 1, pp. 122–134, 2021.

[8] M. Bozzi, S. Germani, L. Minelli, L. Perregrini, and P. de Maagt, "Efficient calculation of the dispersion diagram of planar electromagnetic band-gap structures by the MoM/BI-RME method," *IEEE Transactions on Antennas and Propagation*, vol. 53, no. 1, pp. 29–35, 2005.

[9] P. Baccarelli, S. Paulotto, and C. Di Nallo, "Full-wave analysis of bound and leaky modes propagating along 2D periodic printed structures with arbitrary metallisation in the unit cell," *IET Microwaves, Antennas & Propagation*, vol. 1, no. 1, pp. 217–225, 2007.

[10] M. Petek, J. Rivero, J. A. T. Vásquez, G. Valerio, O. Quevedo-Teruel, and F. Vipiana, "Method of Moments for the Dispersion Modeling of Glide-Symmetric Periodic Structures," *IEEE Trans. Antennas Propag.*, vol. 72, no. 1, pp. 756–766, 2024.

[11] L. Li, D. Werner, J. Bossard, and T. Mayer, "A model-based parameter estimation technique for wide-band interpolation of periodic moment method impedance matrices with application to genetic algorithm optimization of frequency selective surfaces," *IEEE Transactions on Antennas and Propagation*, vol. 54, no. 3, pp. 908–924, 2006.

[12] D. Tihon, S. N. Jha, M. Bodehou, and C. Craeye, "Efficient Tracking of Dispersion Surfaces for Printed Structures Using the Method of Moments," *IEEE Transactions on Antennas and Propagation*, vol. 72, no. 1, pp. 61–74, 2024.

[13] D. Tihon, "Modeling and simulation-based characterization of periodic absorbers for partially coherent fields," Ph.D. dissertation, UC Louvain, 2018. [Online]. Available: https://dial.uclouvain.be/pr/boreal/en/object/boreal%3A200829

[14] S. Rao, D. Wilton, and A. Glisson, "Electromagnetic scattering by surfaces of arbitrary shape," *IEEE Transactions on Antennas and Propagation*, vol. 30, no. 3, pp. 409–418, 1982.

[15] R. Graglia, "On the numerical integration of the linear shape functions times the 3-D Green's function or its gradient on a plane triangle," *IEEE Transactions on Antennas and Propagation*, vol. 41, no. 10, pp. 1448–1455, 1993.